Manipulating the insulating post arrangement in DC-biased AC-iEK devices to improve microparticle separations†

Nuzhet Nihaar Nasir Ahamed, [iD] [a] Carlos A. Mendiola-Escobedo,[b] Victor H. Perez-Gonzalez [iD] *[b] and Blanca H. Lapizco-Encinas [iD] *[a]

There is a growing interest in the advancement of microscale electrokinetic (EK) systems for biomedical and clinical applications, as these systems offer attractive characteristics such as portability, robustness, low sample requirements and short response time. The present work is focused on manipulating the characteristics of the insulating post arrangement in insulator-based EK (iEK) systems for separating a binary mixture of spherical microparticles with same diameter (5.1 μm), same shape, made from the same substrate material and only differing in their zeta potential by ~14 mV. This study presents a combination of mathematical modeling and experimental separations performed by applying a low-frequency alternating current (AC) voltage in iEK systems with 12 distinct post arrangements. These iEK devices were used to systematically study the effect of three spatial characteristics of the insulating post array on particle separations: the horizontal separation and the vertical separation between posts, and introducing an offset to the posts arrangement. Through normalization of the spatial separation between the insulating posts with respect to particle diameter, guidelines to improve separation resolution for different particle mixtures possessing similar characteristics were successfully identified. The results indicated that by carefully designing the spatial arrangement of the post array, separation resolution values in the range of 1.4–2.8 can be obtained, illustrating the importance and effect of the arrangement of insulating posts on improving particle separations. This study demonstrates that iEK devices, with effectively designed spatial arrangement of the insulating post arrays, have the capabilities to perform discriminatory separations of microparticles of similar characteristics.

Introduction

There is a rising need in analytical chemistry applications for developing effective methods for separation of micron-sized particles that can be analogous to the well-established techniques available to isolate nano-sized particles.[1,2] Insulator-based electrokinetic (iEK) microfluidic devices possess the capabilities for assessing a wide range of micron-sized particles, ranging from bacterial to mammalian cells.[3] These systems have attractive characteristics, such as low sample requirements, portability, and low cost. In iEK devices there

are 3-dimensional (3D) insulating structures that distort the distributions of an electric field generated within the device, creating zones of higher and lower field intensity. This enables the unique capability of combining linear and nonlinear EK effects in the same system.[3] Thereby, iEK systems can be advantageously engineered for designing the separation of complex microparticle mixtures.[3,4]

The use of polystyrene-based microparticles as proxies of microorganisms and other important bioparticles of interest, has become a standard practice, as these synthetic microparticles have proved to be excellent platforms for proof-of-concept and development of new separation techniques.[3] Employing polystyrene microparticles speeds up the developing of new separation systems, as they are readily available and exhibit broad distribution of characteristics such as size, shape, surface charge and electrical polarizability.[5,6] Polystyrene particles have thus proven to be excellent surrogates for microorganisms, thereby, opening opportunities for exciting applications in food, health and environmental safety assessments.[6] A crucial element for effective manipulation and separation of

[a]Microscale Bioseparations Laboratory and Biomedical Engineering Department, Rochester Institute of Technology, 160 Lomb Memorial Drive, Rochester, New York, 14623, USA. E-mail: bhlbme@rit.edu
[b]School of Engineering and Sciences, Tecnologico de Monterrey, Monterrey, Nuevo Leon 64849, Mexico. E-mail: vhpg@tec.mx
†Electronic supplementary information (ESI) available: Manipulating the insulating post arrangement in DC-biased AC-iEK devices to improve microparticle separations. See DOI: https://doi.org/10.1039/d3an02160b

microparticles in an iEK system is the arrangement of insulating posts, as it affects the migration of microparticles in the system.[7] Several studies have investigated the effect of the characteristics of the insulating posts on particle trapping and separation.[8–10] A few reports that utilized different shapes for insulating posts such as circles,[11,12] diamonds,[8,11] rectangles,[8] squares,[7] ovals,[13,14] and also a saw-tooth shaped microchannels[9,15,16] for manipulating particle movement established the importance of selecting an adequate design for the insulating post array.[17] The combination of EK with deterministic lateral displacement (DLD), reported for successful separations of bacterial artificial chromosomes,[18] microparticles,[19] and cells,[20] has also been investigated by modifying the characteristics of insulating post array.[21–23] The significance of the geometrical arrangement of insulating posts such as the lateral and longitudinal spacing between posts has also been studied for improving particle trapping performance by applying direct-current (DC) potentials.[7] However, the effect of the geometrical arrangement of posts, along with introduction of an offset arrangement of the posts, on particle manipulation with the aim of separating a binary mixture of similar microparticles by applying low-frequency (<1 kHz) DC-biased alternating-current (AC) potentials is still unknown. A previous study from our group reported an increase in the separation resolution (R_s) of a sample of microparticles from 0.5 to 3.1 by making adjustments to the AC potential,[24] thereby unlocking multiple research opportunities and demanding further investigation of low-frequency AC-iEK systems.

Furthermore, the recent reports on the importance of non-linear electrophoresis (EP_{NL}) in iEK systems,[25–31] have enabled the design of new separation strategies, employing both DC potentials[14,32] and low-frequency AC potentials.[24] Inclusion of EP_{NL} effects is crucial for designing effective iEK separation strategies, as neglecting these effects results in inaccurate predictions of separation performance. In the past, neglecting the effects of EP_{NL} resulted in flawed mathematical models that required correction factors for obtaining agreement with experimental results.[33]

As a first step to further advance the field of low-frequency AC-iEK separation systems, this study is focused on understanding the effect about how the arrangement of the insulating post array affects the separation of a binary mixture of microparticles. This work considers both linear and nonlinear EK phenomena. The polystyrene particles used in this study (both 5.1 μm diameter) only differ in their surface charge as evidenced by a slight (~14 mV) difference in their zeta potential (ζ_P) values. A total of 12 distinct insulating post arrangements were studied with experimentation and numerical modeling with COMSOL Multiphysics. All the spatial arrangements were investigated based on a dimensionless ratio of the horizontal spacing (HS) or vertical spacing (VS) between posts normalized to the particle diameter under investigation (~5 μm). The 12 devices studied here were created with a combination of three values for HS and two values of VS between posts, arbitrarily chosen, in two types of post arrangements – square and offset arrangement. The systematic investigation of the 12

distinct insulating post arrangements utilized a four-step approach, where first, a control separations experiment was performed, followed by studying the effects of varying HS and VS between posts and offsetting the insulating post array for each combination of HS and VS. From each separation experiment, an electropherogram was obtained and the separation performance was evaluated in terms of separation resolution (R_s). The experimental retention time was plotted with respect to normalized horizontal spacing (NHS = HS/5 μm) for different normalized vertical spacing (NVS = VS/5 μm) values to provide trends of retention time for different insulating post arrangements. The results indicated that by carefully devising the spatial arrangements of the insulating post array, separations of microparticles can be performed with the separations resolutions in the range of R_s = 1.43–2.77. This study demonstrates that it is possible to improve the discriminatory capabilities of iEK devices by effectively designing the arrangement of insulating posts in the separation of nano-sized and micro-sized particles, including microorganisms, of similar characteristics, such as shape, size and electric charge.

Theory

Electrokinetic phenomena are categorized as linear and nonlinear based on their dependence on the electric field. Linear EK phenomena are those whose velocity depends linearly on the electric field, $\mathbf{E} = E\hat{\mathbf{a}}_E$ (where $\hat{\mathbf{a}}_E$ is a unit vector with the direction of vector $\mathbf{E}$, having a magnitude E). The linear EK phenomena considered here are linear electroosmotic (EO) flow and linear electrophoresis (EP_L), with the following velocity expressions:

$$\mathbf{v}_{EO} = \mu_{EO}\mathbf{E} = -\frac{\varepsilon_m\zeta_W}{\eta}\mathbf{E} \quad (1)$$

$$\mathbf{v}_{EP,L} = \mu_{EP,L}\mathbf{E} = \frac{\varepsilon_m\zeta_P}{\eta}\mathbf{E} \text{ for } \beta \ll 1, \text{Du} \sim 0,$$
$$\text{and Pe} \ll 1 \text{(weak field regime)} \quad (2)$$

where $\mathbf{v}$ is the velocity, μ_{EO} and $\mu_{EP,L}$ are the linear EO and EP mobilities, respectively. The terms ε_m and η denote the suspending medium permittivity and viscosity, respectively; and the zeta potential of the interfaces between the liquid and the channel wall and the particle are represented by ζ_W and ζ_P, respectively.

The nonlinear EK phenomena considered in this study are nonlinear EP (EP_{NL}) and dielectrophoresis (DEP); they are classified as nonlinear since their velocities exhibit a nonlinear dependence with the magnitude of $\mathbf{E}$. The EP_{NL} velocity ($\mathbf{v}_{EP,NL}$) can be estimated by simple particle tracking velocity experiments (PTV) in a microchannel with constant cross section, once $\mathbf{v}_{EO}$ and $\mathbf{v}_{EP,L}$ are known, by employing the following expression:

$$\mathbf{v}_{EP,NL} = \mathbf{v}_P - \mathbf{v}_{EP,L} - \mathbf{v}_{EO} \quad (3)$$

where $\mathbf{v}_P$ is the overall particle velocity, usually measured experimentally with PTV.

There are several models that describe EP_{NL}, by utilizing the dimensionless applied field strength coefficient (β) and the dimensionless Peclet (Pe) and Dukhin (Du) numbers, to classify the velocity dependence with the magnitude of $\mathbf{E}$. Relevant mathematical expressions for the EP_{NL} velocity ($\mathbf{v}_{EP,NL}$) have been developed only for the two limiting cases of small Pe (Pe $\ll$ 1) and high Pe (Pe $\gg$ 1). For the intermediate cases, there are no formulated expressions. The expressions of $\mathbf{v}_{EP,NL}$ for the two limiting cases are given below,[34–36]

$$\mathbf{v}_{EP,NL}^{(3)} = \mu_{EP,NL}^{(3)} E^3 \hat{\mathbf{a}}_E \text{ for } \beta \sim 1, \text{ arbitrary Du,}$$
$$\text{and Pe} = 1 \text{(moderate field regime)} \tag{4}$$

$$\mathbf{v}_{EP,NL}^{(3/2)} = \mu_{EP,NL}^{(3/2)} E^{3/2} \hat{\mathbf{a}}_E \text{ for } \beta > 1, \text{ Du} \ll 1$$
$$\text{and Pe} \gg 1 \text{(strong field regime)} \tag{5}$$

where $\mu_{(EP,NL)}^{(n)}$ denotes EP_{NL} mobility, and n denotes the dependence of $\mathbf{v}_{EP,NL}$ with the magnitude of $\mathbf{E}$ as evaluated by the operating conditions (see Tables S1 and S2 in ESI†).

The phenomenon of DEP is the result of polarization effects when a particle is exposed to a non-uniform electric field. The expression for $\mathbf{v}_{DEP}$ of a spherical particle is:

$$\mathbf{v}_{DEP} = \mu_{DEP}\nabla E_{rms}^2 = \frac{r_p^2 \varepsilon_m}{3\eta} \text{Re}[f_{CM}]\nabla E_{rms}^2 \tag{6}$$

where r_p is the particle radius, $\text{Re}[f_{CM}]$ is the real part of the Clausius–Mossotti factor, which accounts for polarization effects, and E_{rms} is the root-mean-square value of the electric field magnitude.

Thus, considering all four EK phenomena, the overall particle velocity ($\mathbf{v}_P$) in an iEK device as represented in Fig. 1A becomes:

$$\mathbf{v}_P = \mathbf{v}_{EO} + \mathbf{v}_{EP,L} + \mathbf{v}_{DEP} + \mathbf{v}_{EP,NL}^{(n)} \tag{7a}$$

$$\mathbf{v}_P = \mu_{EO}\mathbf{E} + \mu_{EP,L}\mathbf{E} + \mu_{DEP}\nabla E^2 + \mu_{EP,NL}^{(n)} E^n \hat{\mathbf{a}}_E \tag{7b}$$

The quality of each one of the binary separations carried out in the present study was quantified by assessing the obtained electropherograms in terms of separation resolution (R_s), expressed as follows:

$$R_s = \frac{2(t_{R2,e} - t_{R1,e})}{W_1 + W_2} \tag{8}$$

where W is the width of the peak at the base and $t_{R,e}$ is experimental retention time of each particle type in the post array of the iEK channel (Fig. 1A). The magnitudes of all four EK-phenomena depend on the particle, channel, and suspending media properties, and on the local time-dependent electric field magnitude since a DC biased low-frequency AC signal was employed for all separations.
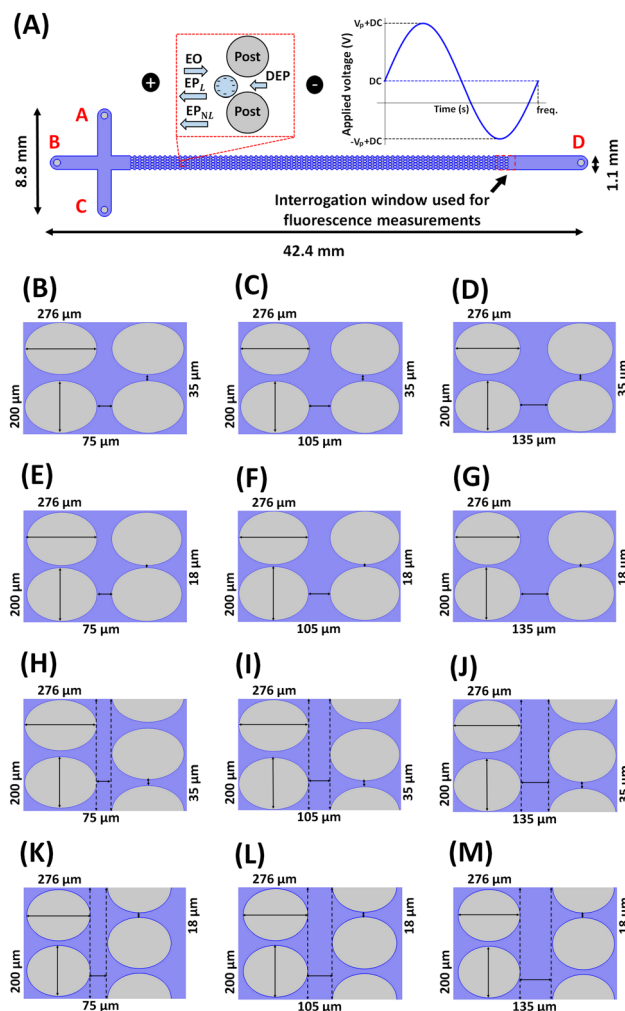

Fig. 1 Illustration of the device designs and the electric stimulation studied in this work. (A) Schematic representation of a complete iEK microchannel, depicting the channel dimensions, and the interrogation window used for fluorescence measurements. The left inset illustrates the four EK forces (EO, EP_L, EP_{NL}, and DEP) acting on negatively charged particles present between the posts in the microchannel. The right inset depicts the DC-biased AC voltage employed in all experiments (300 DC + 800 V_p@1.1 Hz). The microchannel designs employed in this work illustrating different arrangement of the insulating posts with: varying HS between posts – (B) HS-75 μm, VS-35 μm (NHS-15, NVS-7), (C) HS-105 μm, VS-35 μm (NHS-21, NVS-7), (D) HS-135 μm, VS-35 μm (NHS-27, NVS-7), arranged in a square array; varying VS between posts – (E) HS-75 μm, VS-18 μm (NHS-15, NVS-3.6), (F) HS-105 μm, VS-18 μm (NHS-21, NVS-3.6), (G) HS-135 μm, VS-18 μm (NHS-27, NVS-3.6), arranged in a square array; and introducing an offset to the square post array – (H) HS-75 μm, VS-35 μm (NHS-15, NVS-7), (I) HS-105 μm, VS-35 μm (NHS-21, NVS-7), (J) HS-135 μm, VS-35 μm (NHS-27, NVS-7), (K) HS-75 μm, VS-18 μm (NHS-15, NVS-3.6), (L) HS-105 μm, VS-18 μm (NHS-21, NVS-3.6), (M) HS-135 μm, VS-18 μm (NHS-27, NVS-3.6), arranged in an offset array.

Experimental

Suspending medium and microparticles

A 0.2 mM solution of K_2HPO_4 with an addition of 0.05% (v/v) Tween-20 to prevent microparticle clumping, was used as the suspending medium. The conductivity and pH of the medium

were adjusted to 40.7 ± 6 μS cm^{-1} and 7.3 ± 0.5, respectively, by adding 0.1 N KOH solution. These conditions resulted in μ_{EO} of $(4.7 \pm 0.3) \times 10^{-8}$ m^2 V^{-1} s^{-1}, and ζ_W of −60.1 ± 3.7 mV, respectively, which were characterized by averaging the current monitoring experiments performed in different devices with an age of 1–2 days, to avoid aging effects on ζ_W.[37] This EO flow produces a flow rate of −0.37 to 14.76 nL s^{-1} in the microchannel (an expression for estimating the EO flow as a function of the electric field is included in the ESI†). A mixture of two types negatively charged polystyrene microparticles (Magsphere Pasadena, CA, USA) with 5.1 μm diameter at a concentration of 1.2×10^{-8} particles per mL for each particle type was used. The values of ζ_P, $\mu_{EP,L}$ and $\mu_{EP,NL}^{(3)}$ were experimentally assessed for each particle type using PTV experiments (Table 1) employing a channel with a constant cross section.[25,28–30,38] A three-step EK injection process was used to introduce a defined volume of the microparticle mixture into the iEK device.[39]

Microdevices

A total of 12 distinct T-shaped iEK microchannels (Fig. 1, Table S3†) were employed. Each of the 12 iEK devices contained 75 columns of oval-shaped posts that were 276 μm long and 200 μm wide. All devices were made from polydimethylsiloxane (PDMS, Dow Corning, MI, USA) using standard soft lithography techniques[40] After curing, the PDMS casts of the microchannels were gently detached from the mold, inlet and outlet reservoirs were punched, and the device was sealed with a PDMS-coated glass wafer through corona treatment. The depth of all microchannels was 40 μm, and all other channel dimensions are detailed in Fig. 1. To avoid PDMS aging effects on ζ_W,[37] the age of all microdevices used in this work was 1–2 days.

Equipment and software

Electric potentials were applied through four individual platinum wire electrodes labeled A–D (Fig. 1A) by using a high-voltage power supply (Model HVS6000D, LabSmith, Livermore, CA). The experimental sessions were recorded as videos with a digital camera (Lumenera Infinity 2-1C camera model, Infinity Capture application software version 6.5.6) attached to the Zeiss Axiovert 40 CFL (Carl Zeiss Microscopy, Thornwood, NY) inverted microscope.

Experimental procedure

For ensuring stable EO flow, the microchannels were filled with the suspending medium 12–16 h before experimentation. The microparticle suspensions (1 μL) were introduced into reservoir A using a pipette, after which, the four individual platinum wire electrodes were placed into the four reservoirs. The EK injection process using the sequential application of three distinct sets of voltages (i.e., loading, gating, and injection, see Table 2),[39,41] was used to electrokinetically introduce the sample into the microchannel. Injections bias, which allowed the red particles to be injected in a slightly higher proportion, was observed.[41] The 12 distinct insulating post arrangements were systematically studied in four steps. First, a control separations experiment was performed in a device with insulating posts arranged in a square array with a VS and HS of 35 μm and 75 μm, respectively, thereby, having NVS and NHS between posts of 7 and 15, respectively. Second, the effect of HS was studied by employing devices with HS of 105 μm and 135 μm, that is, NHS of 21 and 27, keeping VS and NVS fixed at 35 μm and 7, respectively. Third, the effect of varying the VS was studied by performing experiments with devices with VS = 18 μm, which is, NVS of 3.6. Finally, the effect of offsetting the insulating post array for each combination of HS and VS, also equivalent to combinations of NHS and NVS on the microparticle separation was assessed. All microparticle separations took place under the voltage used for the fourth step of the EK injection process (V_p = 800 V, at 1.1 Hz and a DC bias of 300 V) and relied in the fluid flow generated by electroosmosis (EO flow rate values are given in Table S4†); no external fluid flow is applied. The separation, governed by particle-fluid electrokinetic properties, was considered complete when both particles finished eluting from the post array. The fluorescence signal obtained from each particle eluting peak at the interrogation window (as shown in Fig. 1A) was used to build the electropherograms. All the separations were repeated at least three times to confirm reproducibility (Table S5†), and the two colors of the microparticles were simultaneously measured and discriminated with red, green, blue (RGB) color filters of the camera.

Mathematical modeling

Numerical models of the 12 iEK channels (Fig. 1) were built using COMSOL Multiphysics for predicting the particle retention time ($t_{R,p}$), which were compared to the experimental

Table 1 Characteristics of the microparticles used in this study

ID	Diameter (μm)	ζ_P (mV)	$\mu_{EP,L} \times 10^{-8}$ (m^2 V^{-1} s^{-1})	$\mu_{EP,NL}^{(3)} \times 10^{-17}$ (m^4 V^{-3} s^{-1})
Particle 1, red	5.1 ± 0.2	−20.5 ± 2.2[a]	−1.6 ± 0.2[a]	−2.5 ± 0.6[a,b]
Particle 2, green	5.1 ± 0.2	−34.2 ± 3.7[a]	−2.7 ± 0.3[a]	−1.6 ± 0.1[a,b]

[a] The values of ζ_P, $\mu_{EP,L}$, and $\mu_{EP,NL}^{(3)}$ are specific to the suspending medium employed in this work. [b] The magnitude of $\mu_{EP,NL}^{(3)}$ was estimated at $E = 100$ V cm^{-1} using PTV experiments.

Table 2 Voltage conditions used for EK sample injection and all AC-iEK based separation of the microparticles

Step	Run time (s)	Applied voltage (V) in each reservoir			
		A	B	C	D
Loading (DC)	10	1500	900	0	1000
Gating (DC)	5	2000	2000	200	−100
Injection (DC)	5	200	500	200	0
Separation (AC + DC bias)	800	200	300 (DC) + 800 (V_p)@1.1 Hz	200	0

retention time ($t_{R,e}$) of each particle. The microparticles characteristics listed in Table 1, which were characterized *a priori*, were employed to predict the $t_{R,p}$ values for each particle. Well-resolved peaks ($R_s \geq 1.5$) are obtained when the $\Delta t_{R,p}$ ($\Delta t_R = t_{R1,p} - t_{R2,p}$) value is close to 100 s.[24] The COMSOL model also allowed studying the influence of the insulating post array characteristics on the migration behavior of the microparticles. For more details on the COMSOL model refer to Fig. S1–S3, Table S2.†

Results and discussion

Microparticle separation with a simple device: control experiment

As a control experiment for this study, the separation of the microparticles listed in Table 1 was performed in a simple iEK device with a square array of oval shaped posts with NHS and NVS of 15 and 7, respectively (Fig. 1B). This arrangement of posts was chosen as a control because it is similar to those reported previously by our group,[7,13,42] and to establish a baseline for comparing the separations accomplished with the 11 other proposed insulating post arrangements (Fig. 1C–M). The voltage conditions for all the separations in this study, employing the post arrangements in Fig. 1, are given in Table 2. A numerical model with COMSOL, utilizing the particle properties and voltage conditions in Tables 1 and 2, respectively, was used to predict the $t_{R,p}$ values for each particle for all the separations. Table 3 lists the results obtained with the 12 devices employed in this study, the devices are identified by "IDs" from 1 to 12.

The experimental results of the separation using Device ID #1, where NHS and NVS are 15 and 7, respectively, are presented in Fig. 2A and B. The particles forming "zones" while migrating across the post array can be seen in Fig. 2A, where the red particles are ahead of the green particles. The electropherogram of this separation, shown in Fig. 2B, was built by analyzing the fluorescence signal of the particles as they elute from the post array. As expected from the particle properties (Table 1), the red particles, which have a lower magnitude of ζ_P and $\mu_{EP,L}$, are eluted first at $t_{R1,e}$ = 166.7 s, while the green particles eluted at $t_{R2,e}$ = 261.7 s. This yields a difference in retention times ($\Delta t_{R,e}$) of 95 s, which is very close to the goal of 100 s. Since this separation was carried out under linear EK regime, due to low applied voltages, the difference in surface charge (expressed as ζ_P) is the dominant effect in this separation. The separation resolution R_s of the electropherogram in Fig. 2B was 1.54 (eqn (8)), indicating that the separation was complete ($R_s > 1.5$), resulting in well-resolved peaks. It is important to note that the peaks in the electropherograms have unusual non-Gaussian shapes which is the result of the back-and-forth particle movement due to the DC-biased AC signal, causing the particles to exhibit a negative overall velocity and a velocity magnitude reduction when the signal is minimum and maximum, respectively. Fair agreement between the experimental and predicted values was obtained as the deviations were 11% and 14% for red and green particles, respectively (Table 3). The potential causes for these deviations are discussed at the end of the discussion section.

Effect of varying the horizontal spacing (HS) between posts

The second set of separation experiments investigated the effect of varying the HS between posts arranged in a square array (Fig. 1B and C). The $t_{R,p}$ values for each particle in Device

Table 3 Results of experimental separation and retention time model predictions for all 12 distinct post arrangements: separation resolution (R_s), predicted retention times ($t_{R,p}$) compared with the experimentally obtained retention times ($t_{R,e}$) for the microparticle separations performed

| Device ID and normalized post arrangement	Particle ID	R_s	$t_{R,p}$ (s)	$t_{R,e}$ (s)	Deviation $t_{R,p}$ vs. $t_{R,e}$ (%)
1 NHS-15-NVS-7	1	1.54	147.7	166.7 ± 28.9	11
	2		225.5	261.7 ± 10.4	14
2 NHS-21-NVS-7	1	1.65	176.4	185.7 ± 5.0	5
	2		269.4	283.0 ± 8.7	5
3 NHS-27-NVS-7	1	1.68	210.3	216.7 ± 19.4	3
	2		321.2	344.7 ± 25.3	7
4 NHS-15-NVS-3.6	1	1.67	177.9	209.3 ± 11.9	15
	2		277.7	375.0 ± 14.1	26
5 NHS-21-NVS-3.6	1	2.57	218.7	266.0 ± 26.0	18
	2		334	447.7 ± 25.4	25
6 NHS-27-NVS-3.6	1	2.77	261	270.3 ± 20.4	3
	2		398.7	477.0 ± 32.5	16
7 NHS-15-NVS-7-OFFSET	1	1.55	161.3	180.0 ± 33.6	10
	2		249.2	322.3 ± 28.0	23
8 NHS-21-NVS-7-OFFSET	1	1.52	204.4	218.7 ± 11.0	7
	2		294.4	373.7 ± 17.4	21
9 NHS-27-NVS-7-OFFSET	1	1.55	217.5	232.3 ± 17.8	6
	2		346.9	372.3 ± 32.2	7
10 NHS-15-NVS-3.6-OFFSET	1	1.43	208.2	233.3 ± 30.8	11
	2		317.1	402.3 ± 34.5	21
11 NHS-21-NVS-3.6-OFFSET	1	2.16	223.2	237.3 ± 32.7	6
	2		375.3	477.7 ± 20.7	21
12 NHS-27-NVS-3.6-OFFSET	1	2.44	279.3	288.7 ± 22.0	3
	2		420	519.3 ± 22.6	19
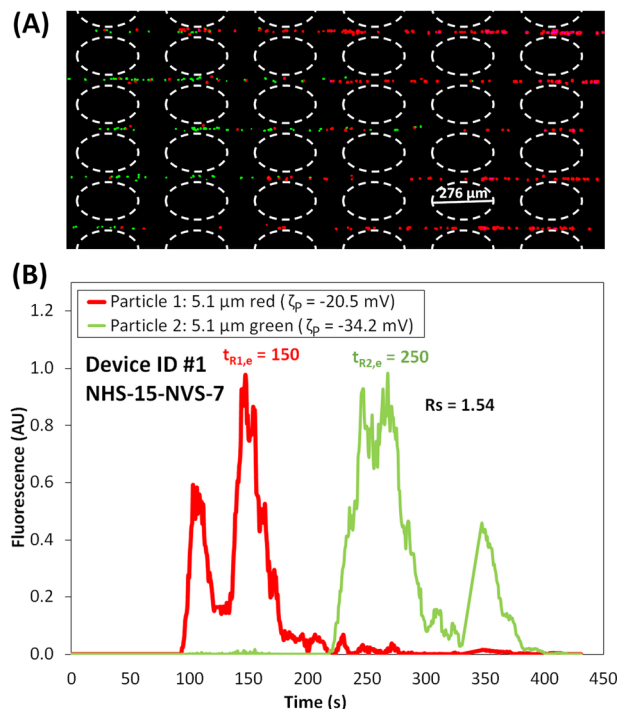
Fig. 2 (A) Image of the microparticles in the post array of the iEK device, where the particles are forming "zones" as the red particles are migrating faster and ahead of the green particles (see ESI Video S1†). (B) Electropherogram of the microparticle separation obtained with NHS = 15 and NVS = 7. The applied potential was V_p = 800 V, at 1.1 Hz and a DC bias of 300 V.

ID #2 and #3 were estimated with COMSOL (Table 3) to compare the designs in terms of the $\Delta t_{R,p}$ values. The experimental separation results are shown in Fig. 3A–B. A linear fitting of $t_{R,e}$ plotted for different NHS, as shown in Fig. 3C, provides a method to extrapolate $t_{R,e}$ values for different values of NHS between posts for a fixed NVS = 7. By comparing the results of varying NHS (Table 3 and Fig. 3C) it can be seen that, as the NHS between posts increases, the retention times (both $t_{R,p}$ and $t_{R,e}$) for both types of particles increase. This can be explained as follows: by increasing the NHS, the maximum magnitude of the local electric field remains almost constant, however, this is not the case for the minimum magnitude of the electric field which decreases with increasing NHS (Fig. S4A†). This affects the overall particle velocity (eqn (7a)) in the inter-column regions of the array. Thereby, as NHS increases, $\mathbf{v}_P$ maximum value remains almost unchanged but $\mathbf{v}_P$ minimum value decreases, resulting in a higher difference in $\mathbf{v}_P$ at higher NHS (Fig. S4B†). Thus, COMSOL simulations provide an explanation for why devices with higher NHS between posts produce better separations in terms higher Δt_R. This is also supported by the experimental results, since R_s increased from R_s = 1.54 to R_s = 1.68 by increasing NHS from 15 to of 27 (Table 3). There is a good agreement (<10% deviations) between experimental results and the model in terms of t_R for both the devices, Device ID #2 and Device ID #3, as shown in (Table 3).
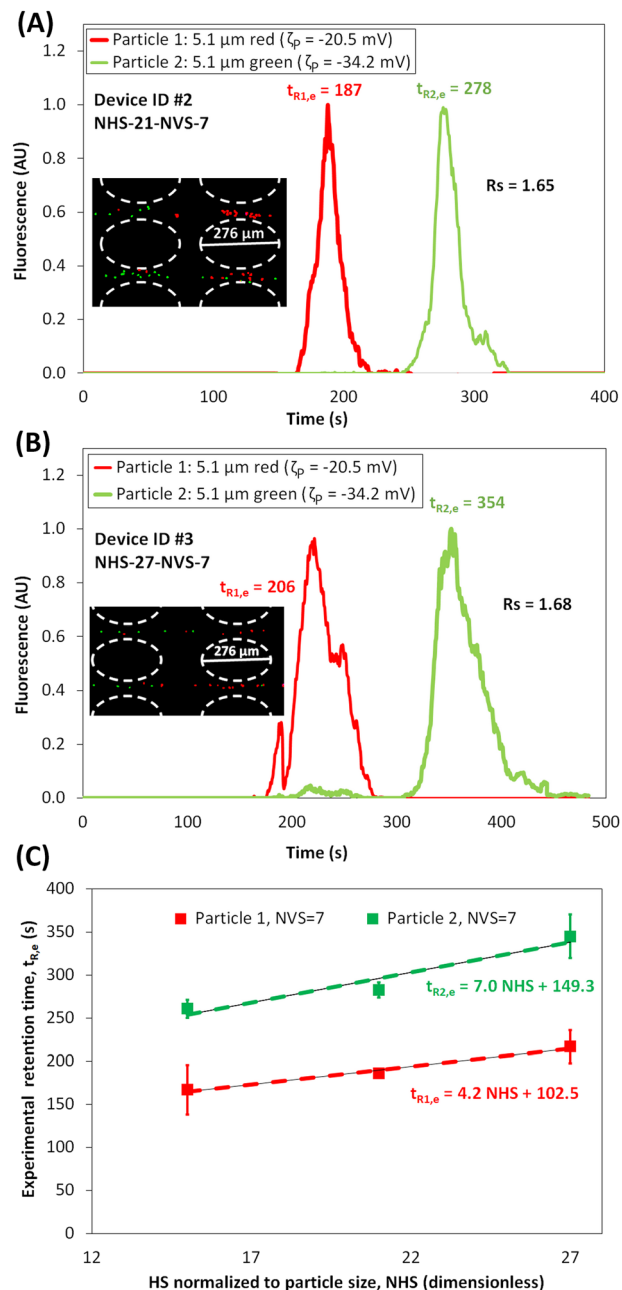

Fig. 3 Assessment of the effect of varying the NHS. (A and B) Electropherograms of the microparticle separation in the microchannel with NHS = 21 and NHS = 27, respectively; NVS = 7 for both devices, and posts were arranged in a square array (see ESI Videos S2 and S3†). Image of the microparticles forming "zones" in the post array, where the red particles migrating faster than the green particles, is shown in the figure inset. The applied potential was V_p = 800 V, at 1.1 Hz and a DC bias of 300 V. (C) Plot of experimental retention time versus the NHS between posts, including a linear fitting of the retention time for both particles at NVS value of 7.

Effect of varying the vertical spacing (VS) between posts

The third set of separations were focused on understanding the effect of the VS between posts arranged in a square array by performing separations in Device IDs #7-#9, which have a

narrower spacing of NVS = 3.6, and NHS of 15, 21 and 27, respectively. Simulations were employed to assess the feasibility of the separations in terms $\Delta t_{R,p}$ values, then, experiments were carried out. The resulting electropherograms are shown in Fig. 4A–C and experimental particle retention times with linear fitting are plotted in Fig. 4D for extrapolating $t_{R,e}$ values at distinct NHS and NVS values. An interesting insight into the effect of the NVS between posts can be gained from the data in Table 3 and the electropherograms (Fig. 2B, 3A, B and 4A–C). The magnitude of Δt_R increases with decreasing NVS, *i.e*, devices become more discriminatory by decreasing the NVS. This is supported by looking at the overall particle velocity for both the particles across a cutline between two posts in Device IDs #1-#6 (Fig. S4B and S5B†). The difference between the overall velocities of the two particles is lower for devices with NVS = 7 (Fig. S4B†) than the difference for devices with NVS = 3.6 (Fig. S5B†). These results also reiterated the effect of the NHS between posts, where more discriminatory separations are obtained at higher NHS values (Fig. S5B†) since lower overall particle velocities are reached at higher NHS. Table 3 shows a clear increase in R_s values when the NVS between posts was decreased from 7 to 3.6 μm, the best separation using Device IDs #1-#6 reached a R_s = 2.77 by combining both optimal features of narrower NVS = 3.6 and higher NHS = 27.

Effect of introducing an offset to the post array

The fourth and final set of separations assessed the effect of introducing an offset to the square array of posts, as shown in Fig. 1H–M. The path of a particle in an offset array is shown in Fig. 5A. The values of numerical model were used to estimate the $\Delta t_{R,p}$ values in Device IDs #7-#12, employing the combination of three values of NHS and two values of NVS and the predicted results indicated that separation would be possible with each device. The electropherograms are shown in Fig. 5C1–E2, where Fig. 5(C–E)1 and 2, correspond to the experimental results of separation with NVS = 7 and 3.6, respectively. Linear fitting of $t_{R,e}$ for different combinations of NHS and NVS in square and offset post array is shown in Fig. 5B1 and B2, respectively. It is important to note that introducing an offset to the square array increased the retention time for both the particles ($t_{R,p}$, and $t_{R,e}$) when compared to their corresponding retention times in a square array of posts, as seen from Table 3. This can be attributed to the fact that the particles are subjected to more frequent distortions in the electric field when the posts are arranged in an offset than with posts arranged in square array. The offset arrangement increases the total path-length of the particles across the device (Fig. 5A), leading to longer elution times. Though the difference in retention times of the particles (Δt_R) increased when an offset was introduced to the post array, the resolution remained either in the same range (R_s = 1.5–1.6 for NVS = 7) or was lower (R_s = 1.4–2.6 for NVS = 3.6) compared to the R_s values obtained with corresponding NVS for square arrays of posts. This can be interpreted by studying the maximum applied electric field plotted for both the particles across two
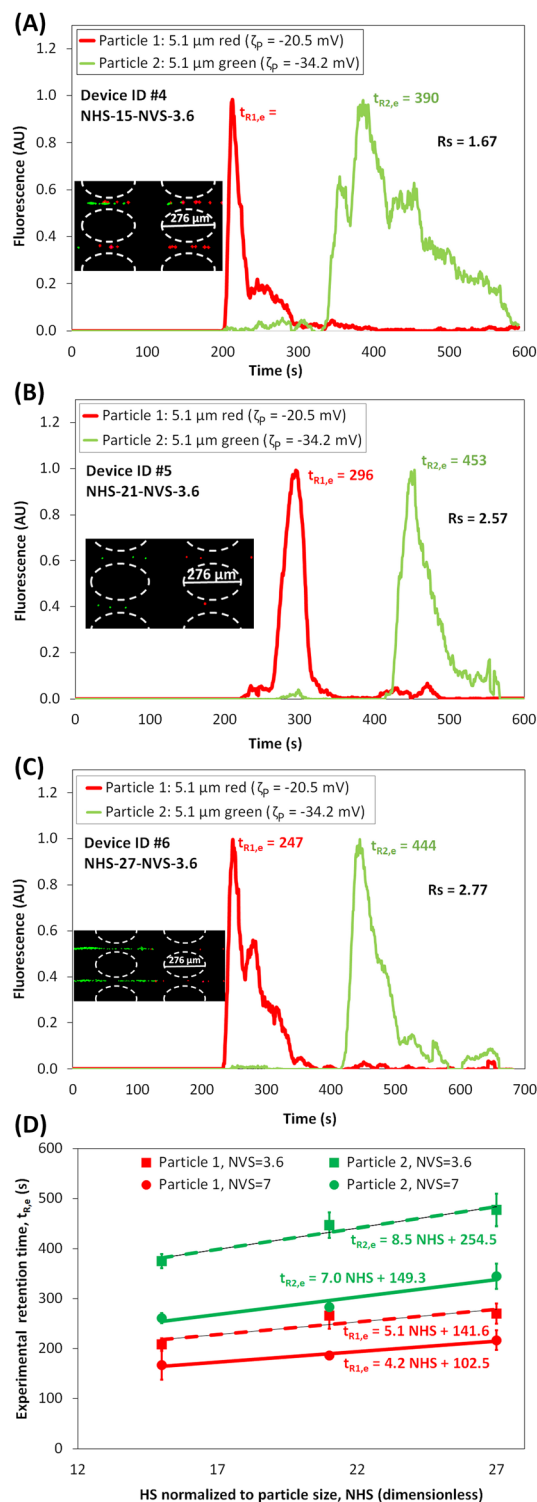

Fig. 4 Assessment of the effect of varying the NVS. (A–C) Electropherograms of the microparticle separation in the microchannel with NVS = 3.6 with NHS = 15, NHS = 21, and NHS = 27, respectively (see ESI Videos S4, S5 and S6†). Image of the microparticles forming "zones" in the post array, where the red particles migrating faster than the green particles, is shown in the figure inset. The applied potential was V_p = 800 V, at 1.1 Hz and a DC bias of 300 V. (D) Plot of experimental retention time *versus* NHS between posts arranged in square array with NVS = 3.6 and NVS = 7, including a linear fitting of the retention time for both particles.
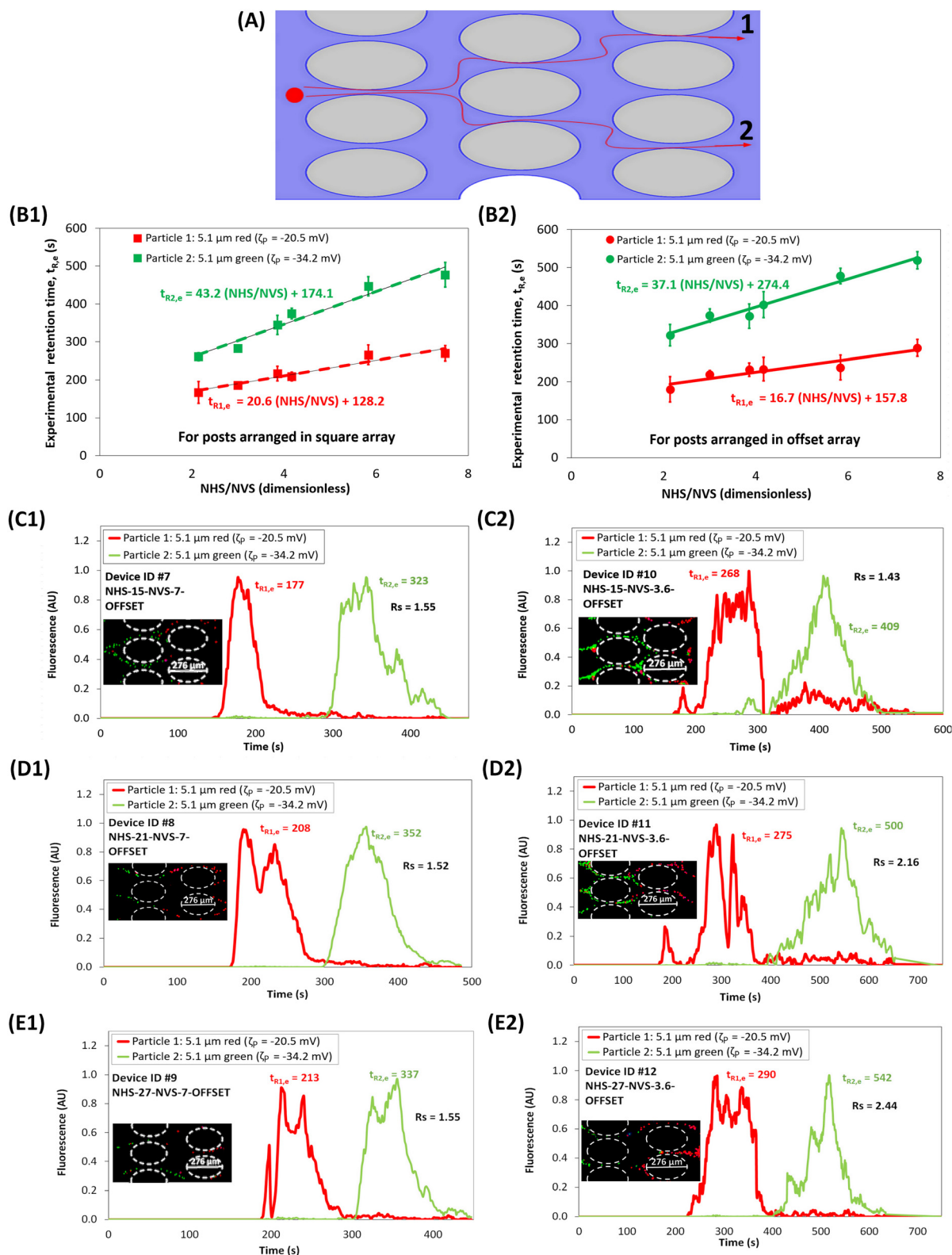
Fig. 5 Assessment of the effect of introducing an offset. (A) Illustration of the path of a particle in an offset array. (B1 and B2) Experimental retention time for both particles plotted with respect to ratio of NHS to NVS, for square and offset array, respectively; including a linear fitting of the retention time for both particles. (C1–E1) Electropherograms of the microparticle separation in microchannels with NHS of 15, 21 and 27, respectively, for devices having offset posts with NVS = 7, (see ESI Videos S7, S8 and S9†) (C2–E2) Electropherograms of the microparticle separation in microchannels with NHS of 15, 21 and 27, respectively, for devices having offset posts with NVS = 3.6, (see ESI Videos S10, S11 and S12†). Image of the microparticles forming "zones" in the post array, where the red particles migrating faster than the green particles, is shown in the figure inset. The applied potential was V_p = 800 V, at 1.1 Hz and a DC bias of 300 V.

cutlines obtained between two posts (Fig. S6†), where one cutline was between offset posts and the other was between non-offset posts. It can be seen that both the maximum and minimum values for the maximum applied electric field across the offset and non-offset posts are almost the same. This explained the reason behind why introducing an offset did not improve R_s for this particular mixture of particles, whose properties are given in Table 1, being separated using the voltage conditions provided in Table 2.

Insights from the mathematical model and potential causes for model deviations

The COMSOL mathematical model was used to predict the overall particle velocity ($\mathbf{v}_P$) for both the particles in all devices, which included the four EK phenomena considered in this study (eqn (7)). All velocity estimations were performed across a horizontal cutline between posts (Fig. S2 and 3†). These modeling results are as expected for a charge-based separation under mainly linear EK regime.[14,24,32] From Table 1, it can be noted that the red particles have a lower magnitude of ζ_P and $\mu_{EP,L}$, which means the EP effects on the red particles (which are toward the inlet) are lower than those on the green particles, thus, the red particles possess a higher overall velocity ($\mathbf{v}_P$) and migrate faster across the post array. All separations in this study were predominantly under the linear EK regime, as seen by the difference in the magnitude of $\mathbf{v}_{EP,L}$ and $\mathbf{v}_{EP,NL}$ (Fig. S7–10†). Since the particles differed by 14 mV in their ζ_P values, using linear EK regime for separation is the best option for the selected particle mixture. Although nonlinear EP effects were not dominant, their presence influenced the overall particle velocity (Fig. S7–10†), thus, it is necessary to consider EP_{NL} to have accurate predictions of particle migration behavior.

Regarding the potential causes for deviations observed in the model predictions, some experimental effects, which are not currently accounted in the model can possibly result in these deviations. For example, the effects of injection bias in EK injection process,[41] electric field distortions caused by the particle themselves,[43] and particle–particle interactions are potential causes for these deviations. Considering these reasons, and the fact that no empirical correction factors were employed,[33] the COMSOL simulation is a valuable tool to be used for the design of challenging separations and to gain insight into the influence of the different device characteristics on the EK phenomena governing the separations.

Conclusions

This research studied the effect of insulating post arrangement of an iEK device on the separation of a binary mixture of particles, differing only in their zeta potentials by ~14 mV, by applying a low-frequency AC voltage. A total of 12 distinct iEK devices were studied to understand the effect of different spatial arrangements of the insulating posts: varying the horizontal and vertical spacing between posts, and introducing an

offset to the post array. This is the first report on understanding the effect of post arrangement on microparticle separations stimulated with a DC biased low frequency AC potential, while considering the effects of nonlinear electrophoresis in the system. Mathematical modeling was used to guide experimentation and to gain an insight on the effect of post arrangement on the performance of the particle separation. The model also allowed gaining an understanding of the dynamics between the linear and nonlinear EK phenomena present in the system. The modeling and experimental retention times had fair agreement, with deviations between 3 to 26%. The quality of separations, assessed in terms of separation resolution (R_s), showed a significant increase in R_s values from 1.5 to 2.7 obtained by carefully designing the posts arrangement. The results from this work illustrate a trend for improving separation resolution by varying the post arrangement, where for the chosen set of particle mixture, increasing the NHS and decreasing the NVS between posts arranged in a square array resulted in an increase in separation resolution. Although the retention time for particles increased in devices with an offset post array, there was no significant improvement in separation resolution for the selected particle mixture, when compared to the corresponding devices with square array of posts. A Linear fitting of the experimental retention time plotted with respect to NHS for different NVS and post arrangements provided trends for the retention time of particles for different configurations of the post array. The main outcome from this work is the insight obtained on spatial arrangement of insulating posts, which is normalized to particle diameter, to enable effective design of insulating post array, for extending microparticle separations to different particle mixtures similar to the one used in this study.

This study, which is a development from our previous report on tuning low frequency AC voltages to improve separation resolution, demonstrates that carefully designed post arrangement combined with low frequency AC signals can allow high discriminatory microparticle separations. This is the first study to experimentally illustrate the effects of varying the horizontal and vertical spacing between insulating posts in iEK microfluidic channels on microparticle separations under DC-biased AC potentials. This study also highlights the effect of increasing the horizontal post separation, which leads to a decrease in the local electric field, increasing the separation resolution of the microparticles. Further, this report characterized in detail microparticle separation resolution in DC-biased AC-iEK systems considering twelve distinct arrangements of insulating posts. The strategy presented here emphasizes that it is feasible to increase the discriminatory capabilities and resolution of separation processes by altering the insulating post arrangement. This first demonstration of the effect of the characteristics of the arrangement of the insulating posts on the separation of microparticles using AC-iEK technique, opens up new research opportunities to explore different insulating post shapes, different geometrical parameters such as post width, length, *etc.*, and optimize the post array for better microparticle separations. Further contributions in this field

will focus on extending the application of AC-iEK systems for separations based on size and tighter charge differences, employing complex mixtures of microparticles and even intact microorganisms.

Author contributions

Conflicts of interest

There are no conflicts to declare.

Acknowledgements

References

1 J. G. Dorsey, *J. Am. Chem. Soc.*, 2010, **132**, 9220–9220.

2 K. Klepárník, *Electrophoresis*, 2015, **36**, 159–178.

3 B. H. Lapizco-Encinas, *Anal. Bioanal. Chem.*, 2022, **414**, 885–905.

4 B. H. Lapizco-Encinas, *Microchim. Acta*, 2021, **188**, 104.

5 M. J. Desai and D. W. Armstrong, *Microbiol. Mol. Biol. Rev.*, 2003, **67**, 38–51.

6 P. Rajapaksha, A. Elbourne, S. Gangadoo, R. Brown, D. Cozzolino and J. Chapman, *Analyst*, 2019, **144**, 396–411.

7 M. A. Saucedo-Espinosa and B. H. Lapizco-Encinas, *J. Chromatogr. A*, 2015, **1422**, 325–333.

8 E. B. Cummings and A. K. Singh, *Anal. Chem.*, 2003, **75**, 4724–4731.

9 K. P. Chen, J. R. Pacheco, M. A. Hayes and S. J. R. Staton, *Electrophoresis*, 2009, **30**, 1441–1448.

10 M. A. Saucedo-Espinosa and B. H. Lapizco-Encinas, *Electrophoresis*, 2015, **36**, 1086–1097.

11 B. H. Lapizco-Encinas, B. A. Simmons, E. B. Cummings and Y. Fintschenko, *Anal. Chem.*, 2004, **76**, 1571–1579.

12 B. H. Lapizco-Encinas, R. V. Davalos, B. A. Simmons, E. B. Cummings and Y. Fintschenko, *J. Microbiol. Methods*, 2005, **62**, 317–326.

13 N. Hill and B. H. Lapizco-Encinas, *Anal. Bioanal. Chem.*, 2020, **412**, 3891–3902.

14 A. Vaghef-Koodehi, O. D. Ernst and B. H. Lapizco-Encinas, *Anal. Chem.*, 2023, **95**, 1409–1418.

15 P. V. Jones, S. J. R. Staton and M. A. Hayes, *Anal. Bioanal. Chem.*, 2011, **401**, 2103–2111.

16 S. J. R. R. Staton, K. P. Chen, T. J. Taylor, J. R. Pacheco and M. A. Hayes, *Electrophoresis*, 2010, **31**, 3634–3641.

17 J. S. Kwon, J. S. Maeng, M. S. Chun and S. Song, *Microfluid. Nanofluid.*, 2008, **5**, 23–31.

18 L. R. Huang, E. C. Cox, R. H. Austin and J. C. Sturm, *Science*, 2004, **304**, 987–990.

19 J. P. Beech, P. Jönsson and J. O. Tegenfeldt, *Lab Chip*, 2009, **9**, 2698–2706.

20 B. Ho, J. Beech and J. Tegenfeldt, *Micromachines*, 2020, **12**, 30.

21 V. Calero, P. Garcia-Sanchez, A. Ramos and H. Morgan, *Biomicrofluidics*, 2019, **13**, 054110.

22 V. Calero, R. Fernández-Mateo, H. Morgan, P. García-Sánchez and A. Ramos, *J. Chromatogr. A*, 2023, **1706**, 464240.

23 B. Ho, J. Beech and J. Tegenfeldt, *Micromachines*, 2020, **11**, 1014.

24 N. Nihaar, N. Ahamed, C. A. Mendiola-Escobedo, O. D. Ernst, V. H. Perez-Gonzalez and B. H. Lapizco-Encinas, *Anal. Chem.*, 2023, **95**, 9914–9923.

25 B. Cardenas-Benitez, B. Jind, R. C. Gallo-Villanueva, S. O. Martinez-Chapa, B. H. Lapizco-Encinas and V. H. Perez-Gonzalez, *Anal. Chem.*, 2020, **92**, 12871–12879.

26 M. Rouhi Youssefi and F. J. Diez, *Electrophoresis*, 2016, **37**, 692–698.

27 S. Tottori, K. Misiunas, U. F. Keyser and D. J. Bonthuis, *Phys. Rev. Lett.*, 2019, **123**, 14502.

28 O. D. Ernst, A. Vaghef-Koodehi, C. Dillis, A. Lomeli-Martin and B. H. Lapizco-Encinas, *Anal. Chem.*, 2023, **95**, 6595–6602.

29 A. Lomeli-Martin, O. D. Ernst, B. Cardenas-Benitez, R. Cobos, A. S. Khair and B. H. Lapizco-Encinas, *Anal. Chem.*, 2023, **95**, 6740–6747.

30 J. Bentor, H. Dort, R. A. Chitrao, Y. Zhang and X. Xuan, *Electrophoresis*, 2023, **44**, 938–946.

31 J. Bentor, A. Malekanfard, M. K. Raihan, S. Wu, X. Pan, Y. Song and X. Xuan, *Electrophoresis*, 2021, **42**, 2154–2161.

32 A. Vaghef-Koodehi, C. Dillis and B. H. Lapizco-Encinas, *Anal. Chem.*, 2022, **94**, 6451–6456.

33 N. Hill and B. H. Lapizco-Encinas, *Electrophoresis*, 2019, **40**, 2541–2552.

34 O. Schnitzer and E. Yariv, *Phys. Fluids*, 2014, **26**, 122002.

35 O. Schnitzer, R. Zeyde, I. Yavneh and E. Yariv, *Phys. Fluids*, 2013, **25**, 052004.

36 R. Cobos and A. S. Khair, *J. Fluid Mech.*, 2023, **968**, A14.

37 M. A. Saucedo-Espinosa and B. H. Lapizco-Encinas, *Biomicrofluidics*, 2016, **10**, 033104.

38 S. Antunez-Vela, V. H. Perez-Gonzalez, A. Coll De Peña, C. J. Lentz and B. H. Lapizco-Encinas, *Anal. Chem.*, 2020, **92**, 14885–14891.

39 A. Miller, N. Hill, K. Hakim and B. H. Lapizco-Encinas, *Micromachines*, 2021, **12**, 628.

40 M. A. Saucedo-Espinosa, A. Lalonde, A. Gencoglu, M. F. Romero-Creel, J. R. Dolas and B. H. Lapizco-Encinas, *Electrophoresis*, 2016, **37**, 282–290.

41 M. C. Breadmore, *Bioanalysis*, 2009, **1**, 889–894.

42 A. LaLonde, A. Gencoglu, M. F. Romero-Creel, K. S. Koppula and B. H. Lapizco-Encinas, *J. Chromatogr. A*, 2014, **1344**, 99–108.

43 M. A. Saucedo-Espinosa and B. H. Lapizco-Encinas, *Anal. Chem.*, 2017, **89**, 8459–8467.